

1 **Global Seasonal Climate Predictability in a Two Tiered**
2 **Forecast System. Part II: Boreal Winter and Spring Seasons**

3 **Haiqin. Li¹ and Vasubandhu Misra^{1, 2, 3, #}**

4 ¹Center for Ocean-Atmospheric Prediction Studies, Florida State University
5 2035 E. Paul Dirac Dr., 200 RM Johnson Bldg., Tallahassee, FL 32306-2840

6 ²Department of Earth, Ocean and Atmospheric Science, Florida State University
7 P.O. Box 3064520, Tallahassee, FL 32306-4520

8 ³Florida Climate Institute, Florida State University,
9 2035 E. Paul Dirac Dr., 200 RM Johnson Bldg., Tallahassee, FL 32306-2840

10

11

Submitted to Climate Dynamics

12

Corresponding author email: vmisra@fsu.edu

12

13 **Abstract**

14 We examine the Florida Climate Institute-Florida State University Seasonal
15 Hindcast (FISH50) skill at a relatively high (50km grid) resolution two tiered
16 Atmospheric General Circulation Model (AGCM) for boreal winter and spring seasons at
17 zero and one season lead respectively. The AGCM in FISH50 is forced with bias
18 corrected forecast SST averaged from two dynamical coupled ocean-atmosphere models.

19 The comparison of the hindcast skills of precipitation and surface temperature
20 from FISH50 with the coupled ocean-atmosphere models reveals that the probabilistic
21 skill is nearly comparable in the two types of forecast systems (with some improvements
22 in FISH50 outside of the global tropics). Furthermore the drop in skill in going from zero
23 lead (boreal winter) to one season lead (boreal spring) is also similar in FISH50 and the
24 coupled ocean-atmosphere models. Both the forecast systems also show that surface
25 temperature hindcasts have more skill than the precipitation hindcasts and that land based
26 precipitation hindcasts have slightly lower skill than the corresponding hindcasts over the
27 ocean.

28

29

29

30 **1. Introduction**

31 The basis for global seasonal climate prediction was initially best illustrated for
32 the boreal winter climate when the El Niño and the Southern Oscillation (ENSO) Sea
33 Surface Temperature (SST) anomalies in the equatorial anomalies are the largest
34 (Bengtsson et al. 1993; Kumar and Hoerling 1995; Shukla 1998; Shukla et al. 2000).
35 These ‘success stories’ spurred the climate modeling community that resulted in
36 significant amount of literature on the impact of slowly varying surface boundary
37 conditions on the genesis, sustenance and demise of several atmospheric climate
38 anomalies (Barnston et al. 1994; Koster et al. 2000; Hoerling et al. 2001; Goddard et al.
39 2001). However these studies highlighted a somewhat arcane and possibly unattainable
40 (in an operational environment) ‘potential’ predictability of the seasonal atmospheric
41 anomalies as they were forced with observed SST. As a result the interest in diagnosing
42 ‘potential’ predictability waned in the community, while efforts to develop and diagnose
43 seasonal predictability of coupled ocean-atmosphere models increased (Stockdale et al.
44 1998; Kirtman 2002, 2003; DeWitt et al. 2005). From these sustained efforts in the last
45 decade or so, there has been a notable improvement in the dynamical ENSO prediction
46 (Saha et al. 2006, 2010; Kirtman and Min 2009; Stockdale et al. 2011; Zhu et al. 2012).
47 Saha et al. (2006) demonstrated for the first time that dynamical coupled ocean-
48 atmosphere models were comparable if not better than statistical forecasts for ENSO. It
49 has now culminated in a massive nation wide co-ordinated effort to develop the National
50 Multi-Model Ensemble (NMME; <http://www.cpc.ncep.noaa.gov/products/ctb/nmme/>)
51 project to harvest the improvements made in the individual modeling centers towards
52 improved seasonal prediction.

53 In this paper we seek to revisit the two-tiered seasonal forecast system for
54 seasonal prediction. The motivation for this is several. One, the improvement in the
55 forecasted SST anomalies from the dynamical prediction systems is worth leveraging.
56 Second, coarseness of the coupled ocean-atmosphere models continues to be an issue. In
57 this study we are investigating seasonal predictability with an Atmospheric General
58 Circulation Model (AGCM) of ~50km grid resolution, which is two to four times higher
59 resolution than the current coupled climate models in the NMME. To meet the growing
60 needs of application studies say for example in hydrology, there is a push towards
61 obtaining climate prediction products at a higher spatial and temporal scales (Bohn et al.
62 2010; Clark and Hay 2004; Shukla et al. 2012). Third, there are some recent studies
63 suggesting that improvement of monsoon climate simulations in climate models is a
64 result of the improved ENSO signal in the model (Delsole and Shukla 2012). Fourth, if
65 the results from this study are promising then it opens the possibility of adding to the
66 NMME effort at a comparatively lower encumbrance with potentially high pay off. Fifth,
67 the basic premise of seasonal climate prediction of slowly varying boundary conditions
68 preconditioning the atmospheric anomalies will always be valid and is worth revisiting
69 periodically to at least assess the progress made in the prediction of the SST anomalies
70 and other boundary conditions. In the next section we explain the experiment design and
71 provide a brief model description. This is followed by the analysis of the results in
72 section 3 followed by summary and conclusions in section 4.

73

74 **2. Experiment Design**

75 The Florida Climate Institute-Florida State University Seasonal Hindcasts at
76 50km grid resolution (FISH50) was implemented to initiate forecasts starting in the
77 boreal winter and integrated through 6 months to end of May of the subsequent year.
78 FISH50 was conducted for the period 1982-2008. Further details of the FISH50
79 experiments are provided in Table 1. FISH50 are two tiered hindcasts, meaning that the
80 Atmospheric General Circulation Model (AGCM) was forced with forecasted SST from
81 another prediction system. The forecasted monthly mean SST anomalies were averaged
82 from two coupled ocean-atmosphere models (CFSv2 [Saha et al. 2010]; CCSM3.0
83 [Kirtman and Min 2009]) which are part of the family of the National Multi-Model
84 Ensemble project (NMME; <http://www.cpc.ncep.noaa.gov/products/ctb/nmme/>). The
85 other coupled ocean-atmosphere models in the NMME project were not utilized as they
86 were not available at the time of conceiving the FISH50 experiments. The multi-model
87 average of the SST anomalies is found to have overall higher prediction skill than any
88 single model (Kirtman and Min 2009). These multi-model averaged SST anomalies are
89 overlaid on observed climatology that contains the seasonal cycle, secular changes and
90 decadal variations. This bias correction of SST anomalies becomes necessary as the
91 systematic errors in CFSv2 and CCSM3.0 in the equatorial Pacific and in the subtropical
92 eastern oceans are grave (Fig. 1). For example, CCSM3.0 displays an equatorial central
93 Pacific cold bias of $\sim 1^{\circ}\text{C}$ in both DJF and MAM seasons. Similarly CFSv2 shows a very
94 large bias (of over 3°C) in the southeastern equatorial Pacific in the MAM season.

95 Obviously in a two-tiered system as FISH50, we have greater flexibility of
96 correcting these systematic errors. However, unlike other flux correction attempts
97 (Drijfhout and Walsteijn 1998; Kirtman et al. 2002; Kirtman 2003), care was taken to

98 exclude the period of forecast (1982-2008) to develop this SST climatology. The
 99 importance and difficulty to adhere to this rule of excluding the FISH50 hindcast period
 100 to develop the observed SST climatology is highlighted in Fig. 2, which shows the
 101 differences in the SST climatology computed in two adjacent 27 year periods of 1955-
 102 1981 and 1982-2008. In both the seasons of DJF and MAM, the systematic difference
 103 between the two periods in the equatorial oceans ranges from about 0.2°C to 0.5°C,
 104 which could be regarded as substantial. In other words, we cannot just use the previous
 105 27 years of mean SST as the observed climatology for the FISH50 hindcast period. As an
 106 alternative we adopted a novel approach following Wu et al. 2009 to compute a time
 107 varying climatology that includes the secular change and decadal variations.
 108 Mathematically, this may be written as:

$$109 \text{ SST}_F = \text{SST}_{OLF} + \text{SSTA}_{MME} + \text{SSTA}_{CYCLE} \text{-----} (1)$$

110 where, SST_F is the forecast SST used to force FISH50 AGCM. SST_{OLF} is the observed
 111 low pass filtered SST. SSTA_{CYCLE} is the monthly climatology of ERSSTv3 (Smith et al
 112 2008) anomaly from 1901-1981. SST_{OLF} is updated at the start of each season. The
 113 monthly mean SST_F is interpolated to daily value following Taylor et al. (2000). The
 114 methodology to obtain SST_{OLF} is explained in Appendix I.

115 The AGCM used in FISH50 essentially follows from the formerly Experimental
 116 Climate Prediction Center’s AGCM at Scripps Institute of Oceanography (Kanamitsu et
 117 al. 2002b; Shimpou et al. 2008) and now referred as the Florida Climate Institute-Florida
 118 State University Global Spectral Model (FGSM). A brief outline of the physics package
 119 used in the FGSM is presented in Table 2. It has 28 vertical (terrain following sigma)
 120 levels. We have however made some subtle but important changes of increasing the

121 resolution to T248 spectral truncation (~50km grid resolution) and replacing the
122 convection scheme from Relaxed Arakawa Schubert (RAS; Moorthi and Suarez 1992) to
123 Kain-Fritsch version 2 (KF2; Kain and Fritsch 1993; Kain 2004) scheme. The motivation
124 for this change can easily be seen in the improvement of the AGCM's seasonal rainfall
125 climatology for DJF and MAM seasons relative to the original version of the model (Fig.
126 3). For these test integrations displayed in Fig. 3, we ran a single ensemble member for
127 12 seasons (1982 to 1993) using the two different convection schemes at T248 spectral
128 truncation forced with SST_F and compared the mean seasonal rainfall over the 12
129 seasons. In Fig. 3, it is clearly seen that KF2 improves the structure of the ITCZ globally
130 relative to RAS. In the latter, the split ITCZ phenomenon is quite apparent especially in
131 the tropical Indian and Pacific Oceans, which is greatly ameliorated in the KF2 version of
132 the FGSM integrations. However, KF2 has a tendency to rain more relative to the RAS
133 integration and observations.

134

135 **3. Results**

136 Since the seasonal hindcasts are global we will compare and validate the results
137 on a larger scale (globally) and let region specific details for subsequent papers. We will
138 in this paper hone in on surface air temperature and precipitation forecasts from FISH50,
139 CCSM3.0 and CFSv2 seasonal hindcasts. The details of the validation datasets used in
140 this section are provided in Table 3.

141

142 *a) SST forcing*

143 The bias in the seasonal mean SST_F (from equation 1; Fig. 4) for both DJF and
144 MAM seasons is greatly reduced compared to the SST bias displayed by either CFSv2 or
145 CCSM3.0 (Fig. 1). The bias in SST_F in Fig. 4 is uniformly in the range -0.5°C to 0.5°C,
146 which is comparably far less than the large errors along the equatorial oceans, subtropical
147 eastern oceans and in the higher latitude storm track regions of both hemispheres in
148 CCSM3.0 and CFSv2 (Fig. 1). Similarly the standard deviation of the mean DJF SST_F
149 (Fig. 5) shows that the variability along the equatorial Pacific Ocean and the Ecuadorian-
150 Peruvian coast is comparable to the other two models. All three show slightly higher
151 variability over the equatorial Pacific in the DJF season, while the mean DJF SST
152 variation in the northern Pacific and in the northern Atlantic is marginally improved in
153 SST_F compared to coupled seasonal hindcasts. In the MAM season, none of the SST
154 forecast products capture the strong variations along the Ecuadorian-Peruvian coast. All
155 of these forecasts contrary to observations exhibit strongest equatorial Pacific SST
156 variations between ~90°W and 160°W. The north Atlantic SST variations in SST_F are
157 slightly improved over the corresponding variations in CFSv2 and CCSM3.0, while over
158 north Pacific it is not so apparent.

159

160 *b) FISH50 climatology*

161 Fig. 6 shows the observed seasonal climatology of precipitation for DJF and
162 MAM seasons along with the corresponding RMSE for each of the three models.
163 Similarly, Fig. 7 show the zonal mean climatological DJF and MAM seasonal mean
164 precipitation from the observations and the three models. From the two figures it is quite
165 apparent that the RMSE of FISH50 is relatively much higher (as a result of erroneously

166 higher precipitation rates) in the tropical latitudes than in either CCSM3.0 and CFSv2
167 hindcasts in both DJF and MAM seasons. In the DJF season, CCSM3.0 displays the least
168 RMSE, while in FISH50 and in CFSv2 the RMSE are especially large over the western
169 Pacific warm pool region, where they tend to rain more than the observations. In FISH50
170 the RMSE is also large over southeastern Africa and southeastern Brazil. In the MAM
171 season the RSME are large in the southern tropics in CCSM3 relative to CFSv2 while
172 still significantly less than that in FISH50. The RMSE in FISH50 in the MAM season
173 continues to be large both over the tropical oceans and over land compared to either
174 CFSv2 and CCSM3.0. The larger tropical RMSE in FISH50 may be highlighting the
175 impact of the absence of the coupled air-sea interactions that could dampen the tropical
176 rainfall activity.

177 The boreal winter and spring climatology of observed surface temperature and the
178 corresponding RMSE from the three models are shown in Fig. 8. The RMSE over Sahara
179 in northern Africa is rather unique in FISH50. Similarly, the errors in northern Russia and
180 Canada are large in FISH50 compared to that in CCSM3.0 and CFSv2. From Fig. 8 it is
181 seen that except for the semi-arid regions and high altitude region (e.g. Tibetan Plateau)
182 the RMSE in FISH50 is comparatively small.

183

184 *c) Deterministic predictability*

185 Deterministic predictability in some ways is a fallacy of climate prediction if it is
186 not complimented with probabilistic assessment of skill (Palmer et al. 2000; Kirtman
187 2003). It is argued that both weather and climate prediction are inherently non-
188 deterministic because of uncertainty in the initial conditions, imperfect and non-linear

189 model that result in chaotic evolution of the climate system. However deterministic skill
190 analysis does provide some (but not complete) insight into the behavior of the forecast
191 system as will be apparent by the conclusion of this paper, when we also compare the
192 models for their probabilistic skill.

193 In Fig. 9 we show the correlation of the seasonal mean precipitation anomalies (of
194 the ensemble mean) from the three model's seasonal hindcasts with the corresponding
195 observed precipitation anomalies for both DJF (zero lead) and MAM (one season lead). It
196 is seen that all three models display expectedly strong positive correlations over the
197 equatorial Pacific Ocean in DJF, which get diminished significantly in the subsequent
198 season in MAM. In fact this diminishment of correlation in the equatorial Pacific is least
199 in FISH50 and most in CCSM3.0. In the DJF season, FISH50 also displays a strong
200 positive correlation over southwestern and southeastern United States, eastern Africa, and
201 over northeastern South America, which are some well known regions for ENSO
202 teleconnections (Ropelewski and Halpert 1986, 1987; AchutaRao and Sperber 2006;
203 Breare et al. 2012). In the CFSv2 seasonal hindcasts, the DJF seasonal precipitation
204 anomalies displays similar but somewhat weaker correlations over these continental
205 regions. But in the CCSM3.0 seasonal hindcasts these regions exhibit barely any
206 significant correlations. As noted earlier, the MAM season comparatively shows weaker
207 correlations than in the DJF season in all three models. In case of FISH50, the positive
208 correlations are shifted to northwestern US and northeast Brazil that are well known
209 again for ENSO teleconnections in the boreal spring season (Ropelewski and Halpert
210 1986; Moura and Hastenrath 2004). Similarly CFSv2 display positive correlations, albeit
211 weaker than FISH50 both over these continental regions and in the equatorial Pacific

212 region. CCSM3.0 seasonal hindcasts, however continue to display the weakest positive
213 correlations.

214 The signal to noise ratio following (Straus and Shukla 2000) is a measure of the
215 forced variance from the boundary conditions (e.g. SST anomalies) to the ensemble
216 spread. A signal to noise ratio close to one (zero) would mean that the forecast is
217 confident (highly uncertain). In Fig. 10 all three models display a high ratio over the
218 equatorial Pacific Ocean for precipitation, which is also the region with the positive
219 correlations (Fig. 9) indicating the overwhelming influence of the underlying SST
220 anomalies on the well predicted atmospheric anomalies. FISH50 and CFSv2 also display
221 a relatively high ratio over southwestern and southeastern United States, eastern Africa
222 and northeastern South America, again likely suggesting the prevailing influence of the
223 ENSO teleconnections in the DJF season. CCSM3.0 on the other hand displays higher
224 ratio over the global equatorial oceans including the Atlantic and the Indian Oceans,
225 where they also display higher positive correlation compared to the other two models in
226 the DJF season (Fig. 9). In the MAM season there is significant reduction in the ratio in
227 all three models, suggesting a relatively higher uncertainty in the ensemble mean
228 anomalies of the seasonal hindcasts. A relatively high signal to noise ratio in the absence
229 of strong positive correlations (in Fig. 9) would suggest that the model is erroneously
230 confident of the forecast anomalies except probably over the semi-arid regions where the
231 correlations of rainfall could be very low and yet the model could be rightfully less
232 uncertain of the forecast anomalies. In this case CCSM3.0 in MAM season shows ample
233 evidence of such erroneous confidence over tropical Indian and Atlantic Oceans.
234 Similarly FISH50 in the MAM season shows erroneously high confidence in the

235 forecasted precipitation anomalies over the western tropical Atlantic Ocean, while CFSv2
236 exhibits the least discrepancy between the ratio and the positive correlation in Fig. 9.

237 A similar correlation of seasonal mean surface temperature anomalies from all
238 three models with corresponding observations is shown in Fig. 11. In the DJF season,
239 FISH50 displays a more extensive positive correlation over Africa, Australia, South
240 America, and North America than either CFSv2 and CCSM3.0. It could be argued in the
241 DJF season that CFSv2 exhibits a larger positive correlation than any other model over
242 equatorial Africa and Arabian Peninsula. The corresponding correlations in CCSM3.0
243 display the least extensive and weakest positive correlations over majority of the
244 continental regions. In the MAM season, FISH50 displays a less extensive positive
245 correlation over Africa (with notable reduction over Sahara), reduction of correlation
246 over Australia and less extensive correlations over United States (with notable positive
247 correlations over southwestern and northwestern United States). The corresponding
248 correlations in CFSv2 are nearly comparable to that in FISH50. However in CCSM3.0
249 there is an appearance of negative correlations from the Arabian Peninsula across central
250 Asia.

251 The signal to noise ratio for seasonal mean surface temperature anomalies (Fig.
252 12) unlike that for precipitation anomalies (Fig. 10) is significantly higher and persistent
253 over both seasons, especially over the oceans. In comparing the ratios in the three
254 models, it is apparent from the figure that FISH50 displays the largest ratios both over
255 land and ocean. However over land, there are more instances of higher signal to noise
256 ratio in areas of weak positive correlations (Fig. 11) in CFSv2 (e.g. over United States,
257 southAsia and Australia. Intriguingly, the signal to noise ratio of the seasonal mean

258 surface temperature anomalies is relatively much smaller in CCSM3.0 over most of the
259 land areas.

260

261 *d) Probabilistic prediction skill*

262 Following Mason and Graham (1999, 2002) we compute the Area under the
263 Relative Operating Characteristic Curve (AROC) to assess the probabilistic skill of the
264 seasonal hindcasts. We have analyzed these skills for the lower, middle and upper terciles
265 for both seasonal mean precipitation and surface land temperature for both DJF and
266 MAM seasons. Unlike the deterministic skill that evaluates the ensemble mean
267 anomalies, AROC is a conditional probability metric that provides the forecast
268 probability for events defined by the user (in this case terciles). The thresholds for the
269 terciles were based on the respective model hindcasts and observations separately. In an
270 operational environment, AROC serves as a useful way to assess a priori an optimal
271 strategy to issue warnings for specific events based on the hindcast performance of the
272 forecast system.

273 In Fig. 13 we show the AROC for FISH50 seasonal precipitation anomalies in
274 DJF and MAM seasons for lower, middle, and upper terciles. In comparison to Fig. 9 it is
275 immediately apparent that more hindcast skill can be harvested through this approach. In
276 DJF season, FISH50 displays much higher skill than climatology for low and upper
277 tercile events over a vast transect of the global tropics including both land and ocean
278 points. Even higher latitude regions display higher skill than climatology in the first
279 season (DJF) of the FISH50 hindcast, which does not seem to be so obvious from Fig. 9.
280 In the subsequent season of MAM (one season lead) the AROC values diminish in their

281 magnitude, but are still sustained (higher than climatology) from the previous season. It is
282 interesting to note that in both seasons, the middle tercile has lesser AROC values than
283 extreme terciles and are also less spatially coherent.

284 Fig. 14 compares the AROC for seasonal precipitation anomalies over global
285 oceans, global tropical oceans, global land, and global tropical land regions between the
286 three models. The following may be noted from Fig. 14:

- 287 • All three models over all these four regions show a reduction of AROC from
288 going from DJF to MAM season for all terciles.
- 289 • All three models display a higher AROC for the extreme terciles than the middle
290 tercile.
- 291 • All three models display higher skill over the oceans than over land in both
292 seasons and for the extreme tercile events.
- 293 • Outside of the global tropics, FISH50 has marginally higher AROC than either of
294 the two models for the high tercile events in the DJF and MAM seasons.
- 295 • For the low tercile events outside of the global tropics, the AROC's are
296 comparable between FISH50 and CFSv2 with significantly lower values for
297 CCSM3.0.
- 298 • For extreme terciles in the global tropics for the DJF season CFSv2 seems to have
299 the highest AROC except for high tercile events over the global tropical land
300 where FISH50 displays the highest values.
- 301 • In the MAM season over global tropical oceans, the AROC values in FISH50 and
302 CFSv2 are comparable while in CCSM3.0 it is significantly less but still above
303 climatology. However over global tropical land regions, all three models display

304 comparable AROC values, with notably less skill than climatology for the middle
305 tercile.

306 Fig. 15 similar to Fig. 13 shows the spatial distribution of the AROC for seasonal
307 mean surface land temperature anomalies from FISH50 for the three terciles. In contrast
308 to Fig. 11, we again see evidence of more probabilistic prediction skill that can be
309 gleaned from FISH50. However, unlike seasonal precipitation anomalies in Fig. 13, the
310 AROC for extreme terciles of surface temperature are higher and more extensive over
311 land especially over Africa, South and North America in both DJF and MAM seasons.
312 Once again we notice that for middle tercile events, the hindcast skill of FISH50 is
313 relatively less than that for the extreme tercile events. Comparing the AROC's across the
314 three models for surface land temperature for global land and tropical land areas (Fig. 16)
315 we notice that in the DJF season the high skills for the extreme tercile events are
316 comparable between CFSv2 and FISH50 with CCSM3.0 showing slightly less skill.
317 However in the MAM season, CFSv2 shows its superiority over the other two models
318 both over global land and global tropical land areas, while AROC in FISH50 remains
319 higher than CCSM3.0 especially outside of the global tropics.

320

321 **4. Summary and conclusions**

322 In part I of this paper we presented the results of the seasonal hindcasts for boreal
323 summer and fall seasons. In this part II of the paper the analysis of seasonal hindcasts for
324 boreal winter and spring seasons are analyzed. At the outset it seems that the two tiered
325 system of FISH50 forced with the bias corrected forecasted SST from single tiered
326 system offers complementary seasonal prediction skill to the coupled ocean-atmosphere

327 forecast systems. A systematic comparison of FISH50 winter and spring seasonal
328 hindcasts with corresponding hindcasts from single tiered systems of CFSv2 and
329 CCSM3.0 reveal the following:

- 330 • The RMSE of precipitation and surface land temperature are higher in FISH50
331 and is least in CCSM3.0. In case of precipitation, the RMSE are larger in the
332 tropical latitudes while for surface land temperature it appears at higher latitudes.
- 333 • Skillful boreal winter (spring) season rainfall anomalies over southeastern and
334 southwestern United States, northeastern South America and eastern Africa
335 (northwestern United States) appears to be a forced signal as they appear in the
336 deterministic skill analysis. It may be noted that in all these regions FISH50
337 displays the largest skill compared to either CFSv2 and CCSM3.0.
- 338 • Similarly the correlations of the seasonal surface land temperature anomalies from
339 the seasonal hindcasts and corresponding observations are most extensive over
340 Africa, South and North America in FISH50 relative to the other two models in
341 both boreal winter and spring seasons.
- 342 • The probabilistic skill analysis reveals that in all three models there is more
343 forecast skill to be gleaned for the extreme tercile events in both seasons (DJF and
344 MAM) and for both variables (precipitation and surface land temperature), while
345 for the middle tercile events CFSv2 and FISH50 (CCSM3.0) are marginally
346 better (worse) than climatology.

347 The changes made to the convection scheme, the increase of resolution to T248
348 spectral truncation (~50km grid resolution), and use of the unique way of bias correction
349 of dynamically forecasted SST may all have contributed to the displayed fidelity of

350 FISH50. The deterioration of the skill from DJF to MAM season across all three models
351 suggests some further investigation is required to discern the role of increasing lead time
352 and the inherent seasonal nature of the climate system (e.g. the spring predictability
353 barrier). Nonetheless, this study shows that coupled forecast systems may have reached a
354 stage, wherein the forced forecast systems like FISH50 could be used to exploit the
355 superiority of the SST forecasts to glean further seasonal prediction skill. The advantage
356 of stand alone AGCM's is that it is computationally less demanding to raise their
357 resolution to levels that can then be more meaningful for application in other fields (e.g.
358 hydrology, agriculture etc.). FISH50 in this study unlike in the boreal summer and fall
359 seasons (in part I of the paper) do not seem to show as much of a benefit over the much
360 coarser dynamical coupled ocean-atmosphere seasonal forecasts. However, it should be
361 mentioned that all three models display hindcast skills, which is better than climatology.

362

363 *Acknowledgements*

364 This paper is dedicated to the memory of Dr. Masao Kanamitsu, without whose
365 pioneering development of the FISH50 AGCM, this work would not have been possible.
366 We also acknowledge the help of Dr. Zhaohua Wu who provided us the methodology and
367 the data for the bias corrected SST (SST_{OLF}). We thank Mr. Steven DiNapoli for making
368 Figs. AII.1, AII.2, AII.3. This work was supported by grants from NOAA
369 (NA12OAR4310078, NA10OAR4310215, NA11OAR4310110), USGS (06HQGR0125),
370 and USDA (027865). All computations for this paper were done on the computational

371 resources provided by the Extreme Science and Engineering Discovery Environment
372 (XSEDE) under TG-ATM120017 and TG-ATM120010.

373

374

374

375 **Appendix I: The methodology for computing SST_{OLF}**

376 SST_{OLF} is the observed low pass filtered SST in equation 1 of the main text.

377 SST_{OLF} is used to replace the model climatology of SST in the process of bias correction.

378 Unlike other bias correction techniques SST_{OLF} contains low frequency variations and the

379 secular climate change signal. Using Extended Reynolds SST version 3 (ERSSTv3;

380 Smith et al. 2008) at 2° resolution (SSTO) for the period 1870-2008 we first conduct a

381 Multi-dimensional Ensemble Empirical Model Decomposition (MEEMD) analysis

382 following Wu et al. (2009). MEEMD is a multi-dimensional (in space) data adaptive time

383 series analysis of Ensemble Empirical Mode Decomposition (EEMD; Wu and Huang

384 2009). EEMD seeks to determine the intrinsic modes of oscillations in the data on the

385 principle of local scale separation, which are called Intrinsic Mode Functions (IMFs).

386 Although the decomposition in MEEMD does not make use of information on spatial

387 coherence of the dataset, the obtained evolution of SST_{OLF} are both temporally and

388 spatially coherent (true to its low frequency feature), which exhibits large spatial scale

389 features when the SST_{OLF} is mapped on a global grid:

390

391

391

392 Appendix II: Comparison of FISH50 with the other National Multi-Model

393 Ensemble (NMME) models

394 The NMME project (<http://www.cpc.ncep.noaa.gov/products/ctb/nmme/>) hosted by

395 International Research Institute for Climate and Society, Columbia University and

396 maintained in real time at the NCEP Climate Prediction Center

397 (<http://www.cpc.ncep.noaa.gov/products/NMME/>) are eight single tiered coupled ocean-

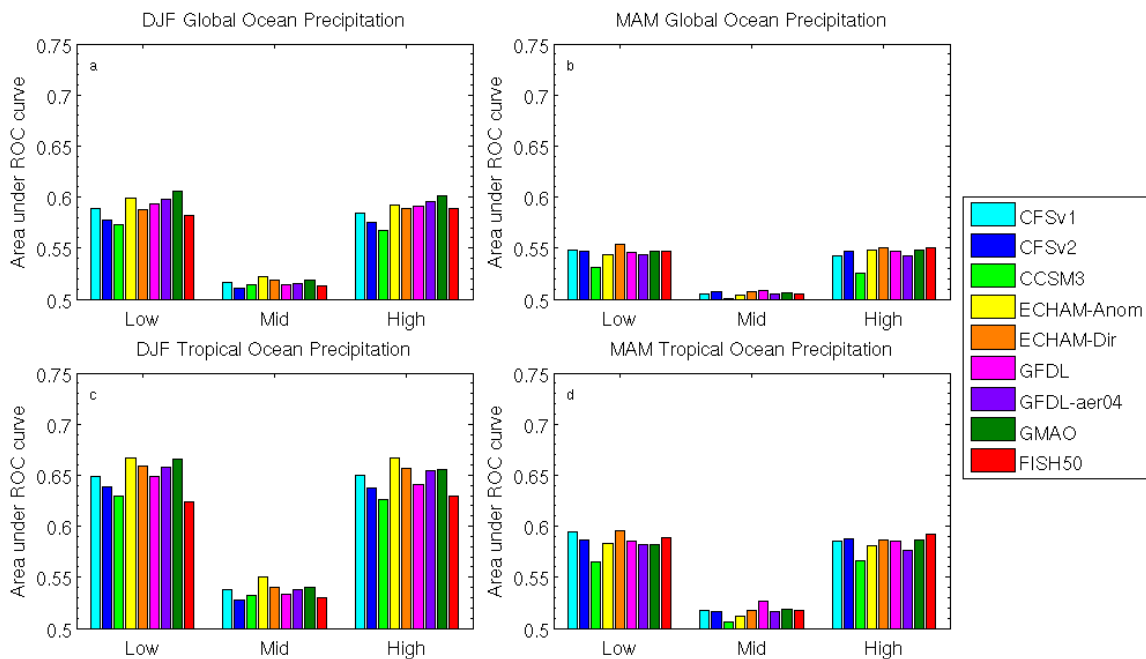
398 atmosphere models, which have conducted extensive seasonal hindcasts over the same

399 time period as FISH50 and more. In fact NMME models have completed seasonal

400 hindcasts for several lead times throughout the year and here we compare the AROC for

401 tercile events of seasonal mean surface land temperature and precipitation from FISH50

402 with the corresponding hindcasts of the NMME.

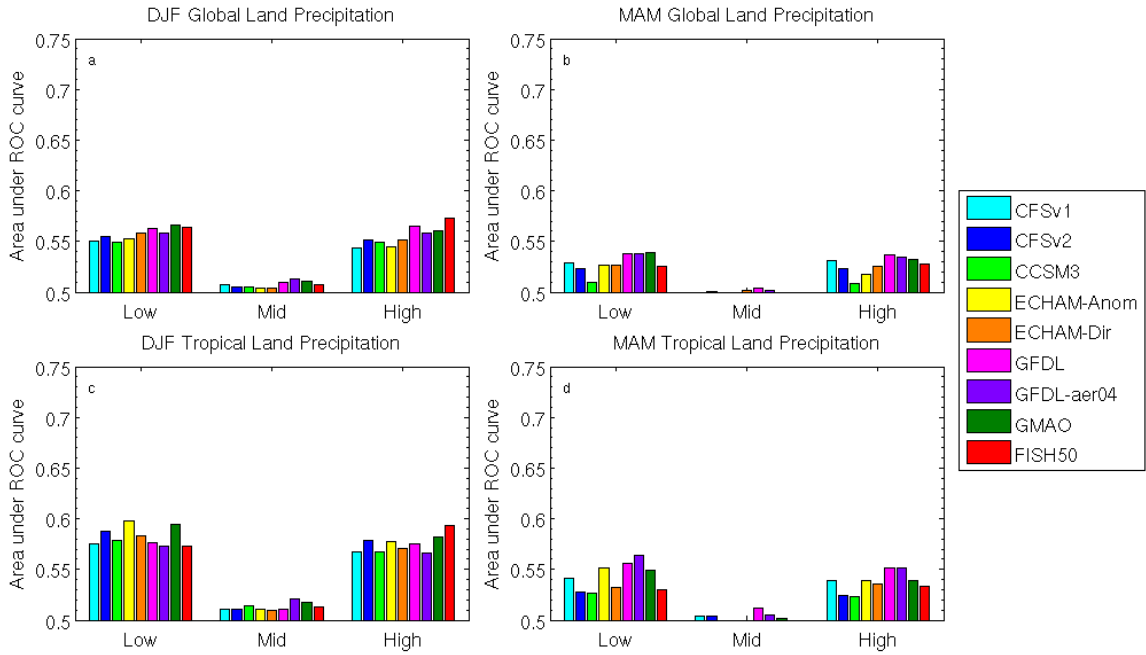


403

404 Figure AII.1: AROC averaged over global oceans for (a) DJF, (b) MAM, over tropical

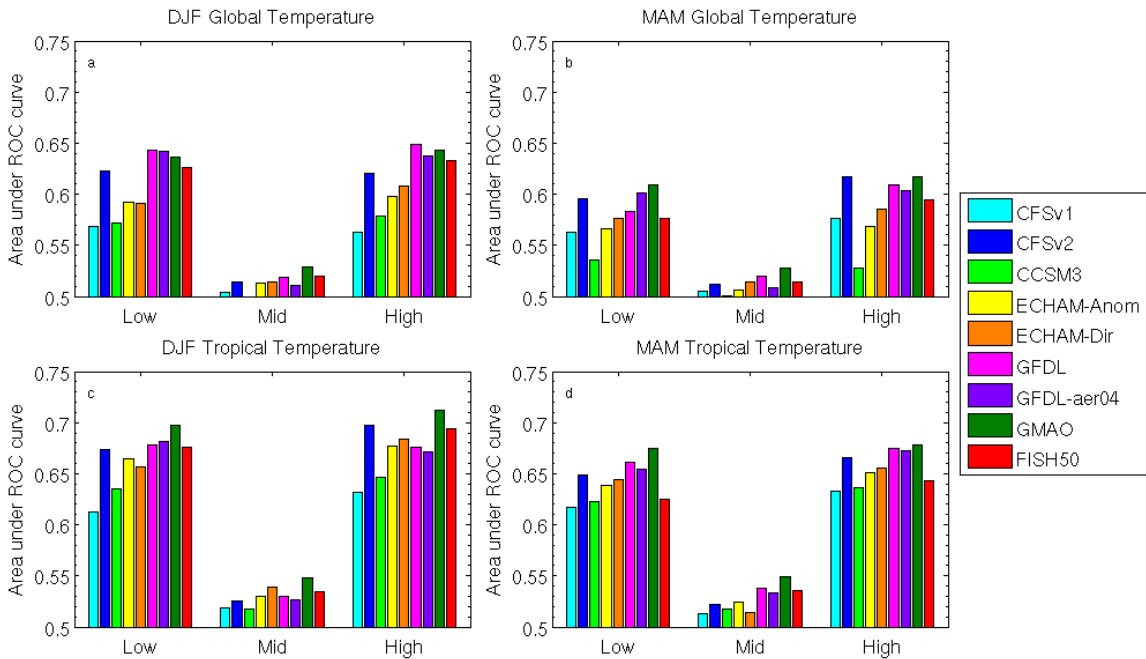
405 oceans for (c) DJF, and (d) MAM for low, middle, and upper terciles of NMME and

406 FISH50 precipitation.



407

408 Figure AII.2: AROC averaged over global land for (a) DJF, (b) MAM, over tropical land
 409 for (c) DJF, and (d) MAM for low, middle, and upper terciles of NMME and FISH50
 410 precipitation.
 411



412

413 Figure AII.3: Same as Fig. AII.2 but for surface land temperature.
 414

414

414 **References**

415

416 AchutaRao K.M., and K.R. Sperber (2006) ENSO simulation in coupled ocean-
417 atmosphere models: Are the current models better? *Climate Dynamics*
418 doi:10.1007/s00382-006-0119-7

419 Alpert J. C., M. Kanamitsu, P. M. Caplan, J. G. Sela, G. H. White, and E. Kalnay (1988)
420 Mountain induced gravity wave drag parameterization in the NMC medium-range
421 model. Preprints, Eighth Conf. on Numerical Weather Prediction, Baltimore, MD.
422 Amer Meteor Soc: 726-733

423 Barnston, A. G., and Coauthors (1994) Long lead seasonal forecasts-where do we stand?
424 Bull Am Meteorol Soc 75: 2097-2114

425 Bengtsson L, U. Schlese, E. Roeckner (1993) A two-tiered approach to long-range
426 climate forecasting. *Science* 261: 1026-1029

427 Bohn, T. J., Sonessa, M. Y., and Lettenmaier, D. P. (2010) Seasonal Hydrologic
428 Forecasting: Do multi-model ensemble averages always yield improvements in
429 forecast skill? *J Hydrometeorol* 11:1358-1372

430 Chen F, Dudhia J (2001) Coupling and advanced land surface-hydrology model with the
431 Penn State- NCAR MM5 modeling system. Part I: Model implementation and
432 sensitivity. *Mon Wea Rev* 129:569-585

433 Chou M-D (1992) A solar radiation model for use in climate studies, *J Atmos Sci*
434 49:762-772

435 Chou M-D, Lee K-T, Tsay S-C, Fu Q (1996) Parameterization for cloud long wave
436 scattering for use in atmospheric models. *J Climate* 12:159-169

437 Clark M. P., and L. E. Hay (2004) Use of medium-range numerical weather prediction
438 model output to produce forecasts of stream-flow. *J. Hydrometeor* 5: 15–32

439 DelSole T., and J. Shukla (2012) Climate models produce skillful predictions of Indian
440 summer monsoon rainfall. *Geophys Res Lett* 39: doi:10.1029/2012GL051279

441 DeWitt D. G. (2005) Retrospective Forecasts of Interannual Sea Surface Temperature
442 Anomalies from 1982 to Present Using a Directly Coupled Atmosphere–Ocean
443 General Circulation Model. *Mon Wea Rev* 133: 2972–2995

444 Drijfhout S. S., Fred H. Walsteijn (1998) Eddy-Induced Heat Transport in a Coupled
445 Ocean–Atmospheric Anomaly Model. *J Phys Oceanogr* 28: 250–265

446 Ek MB, Mitchell KE, Lin Y, Rogers E, Grunmann P, Koren V, Gayno G, Tarpley JD
447 (2003) Implementation of Noah land surface model advances in the National Centers
448 for Environmental Prediction operational mesoscale 437 Eta model. *J Geophys Res*
449 108: 8851, doi: 10.1029/2002JD003296

450 Goddard, L., S. J. Mason, S. E. Zebiak, C. F. Ropelewsky, R. Basher, and M. A. Cane
451 (2001) Current approaches to seasonal-to-interannual climate predictions. *Int J*
452 *Climatol* 21: 1111–1152

453 Hoerling M. P., J. W. Hurrell, and T. Xu (2001) Tropical Origins for Recent North
454 Atlantic Climate Change. *Science* 292: 90-92

455 Hong S.-Y., and H.-L. Pan (1996) Nonlocal boundary layer vertical diffusion in a
456 medium-range forecast model. *Mon Wea Rev* 122: 3-26

457 Huang NE, Wu Z, Pinzo'n JE, Parkinson CL, Long SR, Blank K, Gloersen P, Chen X
458 (2009b) Reductions of noise and uncertainty in annual global surface temperature
459 anomaly data. *Adv Adapt Data Anal* 1:447-460

460 Kain J. S., and J. M. Fritsch (1993) Convective parameterization for mesoscale models:
461 The Kain-Fritsch scheme. *The Representation of Cumulus convection in Numerical*
462 *Models. Meteor. Monogr. No. 46, Amer Meteor Soc* : 165-170

463 Kain J. S. (2004) The Kain-Fritsch Convective Parameterization: An update. *J Appl*
464 *Meteor* 43:170-181

465 Kanamitsu, M., and Coauthors, 2002: NCEP Dynamical Seasonal Forecast System 2000.
466 *Bull Amer Meteor Soc* 83: 1019-1037

467 Kanamitsu, M., W. Ebisuzaki, J. Wollen, S-K Yang, J.J. Hnilo, M. Fiorino, and G. L.
468 Potter (2002) NCEP-DOE AMIP-II Reanalysis. *Bull Amer Meteor Soc* 83: 1631-
469 1643

470 Kirtman B. P., Y. Fan, and E. K. Schneider (2002) The COLA global coupled and
471 anomaly coupled ocean-atmosphere GCM. *J Climate* 15: 2301-2320

472 Kirtman, B. P. (2003) The COLA anomaly coupled model: Ensemble ENSO prediction.
473 *Mon Wea Rev* 131: 2324-2341

474 Kirtman, B. P., and D. Min (2009) Multimodel Ensemble ENSO Prediction with CCSM
475 and CFS. *Mon Wea Rev* 137: 2908-2930

476 Koster, R. D., M. J. Suarez, and M. Heiser (2000) Variance and predictability of
477 precipitation at seasonal-to-interannual time scales. *J Hydrometeorol* 1: 26–64.

478 Kumar A, Hoerling MP (1995) Prospects and limitations of seasonal atmospheric GCM
479 predictions. *Bull Amer Meteorol Soc* 76:335–345

480 Mason S. J., and N. E. Graham, 1999: Conditional probabilities, relative operating
481 characteristics, and relative operating levels. *Weather and Forecasting* 14: 713-725

482 Mason S. J., and N. E. Graham, 2002: Areas beneath the relative operating characteristics
483 (ROC) and levels (RROL) curves: statistical significance and interpretations. *Quart J*
484 *Royal Meteorol Soc* 128: 2145-2166

485 Mitchell T. D., and P. D. Jones, 2005: An improved method of constructing a database of
486 monthly climate observations and associated high-resolution grids. *Int J Climatol* 25:
487 693–712

488 Moorthi S., and M. J. Suarez (1992) Relaxed Arakawa-Schubert. A Parameterization of
489 Moist Convection for General Circulation Models. *Mon Wea Rev* 120: 978-1002

490 Moura AD, and Hastenrath S (2004) Climate prediction for Brazil's Nordeste:
491 Performance of empirical and numerical modeling methods. *J Climate* 17: 2667–
492 2672

493 Palmer TN, Branković C, and Richardson DS (2000) A probability and decision-model
494 analysis of PROVOST seasonal multi-model ensemble integrations. *Quart J Roy Met*
495 *Soc* 126: 2013-2034

496 Ropelewski CF, Halpert MS (1986) North American precipitation and temperature
497 patterns associated with the El Nino/Southern Oscillation (ENSO). *Mon Wea Rev*
498 114:2352–2362

499 Ropelewski CF, Halpert MS (1987) Global and regional scale precipitation patterns
500 associated with the El Niño/Southern Oscillation. *Mon Wea Rev* 115:1606–1626

501 Saha S., and Coauthors (2006) The NCEP Climate Forecast System. *J Climate* 19: 3483–
502 3517

503 Saha S. and Coauthors (2010) The NCEP Climate Forecast System Reanalysis. *Bull*
504 *Amer Meteor Soc* 91: 1015-1057

505 Shimpo, A., M. Kanamitsu, S. F. Iacobellis, and S.-Y. Hong (2008) Comparison of Four
506 Cloud Schemes in Simulating the Seasonal Mean Field Forced by the Observed Sea
507 Surface Temperature. *Mon Wea Rev* 136: 2557-2575

508 Shukla J (1998) Predictability in the midst of chaos: A scientific basis for climate
509 forecasting. *Science* 282: 728-731

510 Shukla J., J. Anderson, D. Baumhefner, C. Brankovic, Y. Chang, E. Kalnay, L. Marx, T.
511 Palmer, D. A. Paolino, J. Ploshay, S. Schubert, D. M. Straus, M. Suarez, J. Tribbia,
512 (2000) Dynamical Seasonal Prediction. *Bull Amer Meteor Soc* 81: 2593-2606

513 Shukla,J., T.N. Palmer, R. Hagedorn, B. Hoskins, J. Kinter, J. Marotzke, M. Miller, and
514 J. Slingo (2010) Towards a New Generation of World Climate Research and
515 Computing Facilities. *Bull Amer Meteor Soc* 91: 1407-1412

516 Slingo J. M. (1987) The development and verification of a cloud prediction model for the
517 ECMWF model. *Quart J Roy Meteor Soc* 113: 899-927

518 Smith T. M., R. W. Reynolds, T. C. Peterson, and J. Lawrimore (2008) Improvements to
519 NOAA's Historical Merged Land-Ocean Surface Temperature Analysis (1880-2006).
520 *J. Climate* 21: 2283-2296

521 Stockdale TN, Anderson DLT, Alves JOS, Balmaseda MA (1998) Global seasonal
522 rainfall forecasts using a coupled ocean-atmosphere model. *Nature* 392: 370-373

523 Stockdale TN, Anderson DLT, Balmaseda MA, Doblas-Reyes FJ, Ferranti L, Mogensen
524 K, Palmer TN, Molteni F, Vitart F (2011) ECMWF seasonal forecast system 3 and its
525 prediction of sea surface temperature. *Clim Dyn*. doi:10.1007/s00382-010-0947-3

526 Straus D. M. and J. Shukla (2000) Distinguishing between the SST-forced variability and
527 internal variability in mid-latitudes: Analysis of observations and GCM simulations.
528 *Quart J Royal Meteor Soc* **126**: 2323-2350

529 Wu, Z., and N. E Huang, 2009: Ensemble Empirical Mode Decomposition: a noise-
530 assisted data analysis method. *Advances in Adaptive Data Analysis*. **1**, 1-41.

531 Wu, Z., N. E. Huang, and X. Chen, 2009: The multi-dimensional Ensemble Empirical
532 Mode Decomposition method. *Advances in Adaptive Data Analysis*, **1**, 339-372.

533 Wu Z., N. E. Huang, J. M. Wallace, B. V. Smoliak, and X. Chen (2011) On the time-
534 varying trend in global-mean surface temperature. *Clim Dyn* 37: 759-773

535 Xie and Arkin (1997) Global Precipitation: A 17-year monthly analysis based on gauge
536 observations, satellite estimates, and numerical model outputs, Bull Ameri Meteorol
537 Soc 78: 2539-2558

538 Zhu J., B. Huang, L. Marx, J. L. Kinter III, M. A. Balmaseda, R.-H. Zhang, and Z.-Z.
539 Hu (2012) Ensemble ENSO hindcasts initialized from multiple ocean
540 analyses. Geophys Res Lett 39: L09602, doi:10.1029/2012GL051503

541

541
542
543

Table 1: FISH50 Experiment Design

544

Seasonal hindcast feature	Detail					
Length of each seasonal hindcast integration	6 months					
Number of ensemble members for each seasonal hindcast	6 (E1, E, E3, E4, E5, E6)					
Seasonal hindcast period	1982-2008					
Seasonal hindcast start date	E1	E2	E3	E4	E5	E6
	28 Nov,	29 Nov,	30	01 Dec,	02	03
	0000	0000	Nov,	0000	Dec,	Dec,
	UTC	UTC	0000	UTC	0000	0000
			UTC		UTC	UTC
Atmospheric initial conditions	Borrowed for subsequent days from 28 Nov to 03 Dec from the NCEP-DOE reanalysis (Kanamitsu et al. 2002) for each ensemble member and interpolated to the FISH50 grid					
Land initial conditions	Interpolated from NCEP-DOE reanalysis and kept identical in all ensemble members for each season					

545
546
547

547

548 **Table 2: A brief outline of the physics of the FISH50 AGCM**

549

550

Parameterization	Reference
Cumulus parameterization	Kain-Fritsch (Kain and Fritsch 1993; Kain 2004)
Shallow convection	Tiedtke scheme (Tiedtke 1983)
Boundary layer	Nonlocal scheme (Hong and Pand 1996)
Land surface	NOAH (Chen and Dudhia 2001; Ek et al 2003)
Gravity wave drag	Pierrehumbert (Alpert et al 1988)
Shortwave radiation	M.-D. Chou (Chou and Lee 1996)
Longwave radiation	M.-D. Chou (Chou and Suarez 1994)
Clouds	Slingo 1987

551

552

553

554

554 **Table 3: Details of the validation datasets used**
 555

556
 557

Global Dataset Name	Variable	Reference	Resolution	Period Available
Climate Prediction Center Merged Analysis of Precipitation (CMAP)	Precipitation	Xie and Arkin (1997)	2.5°x2.5°	1979-present
Climate Research Unit version 3 (CRUv3)	Surface temperature	Mitchell and Jones (2005)	0.5°x0.5°	1900-present

558

559

560

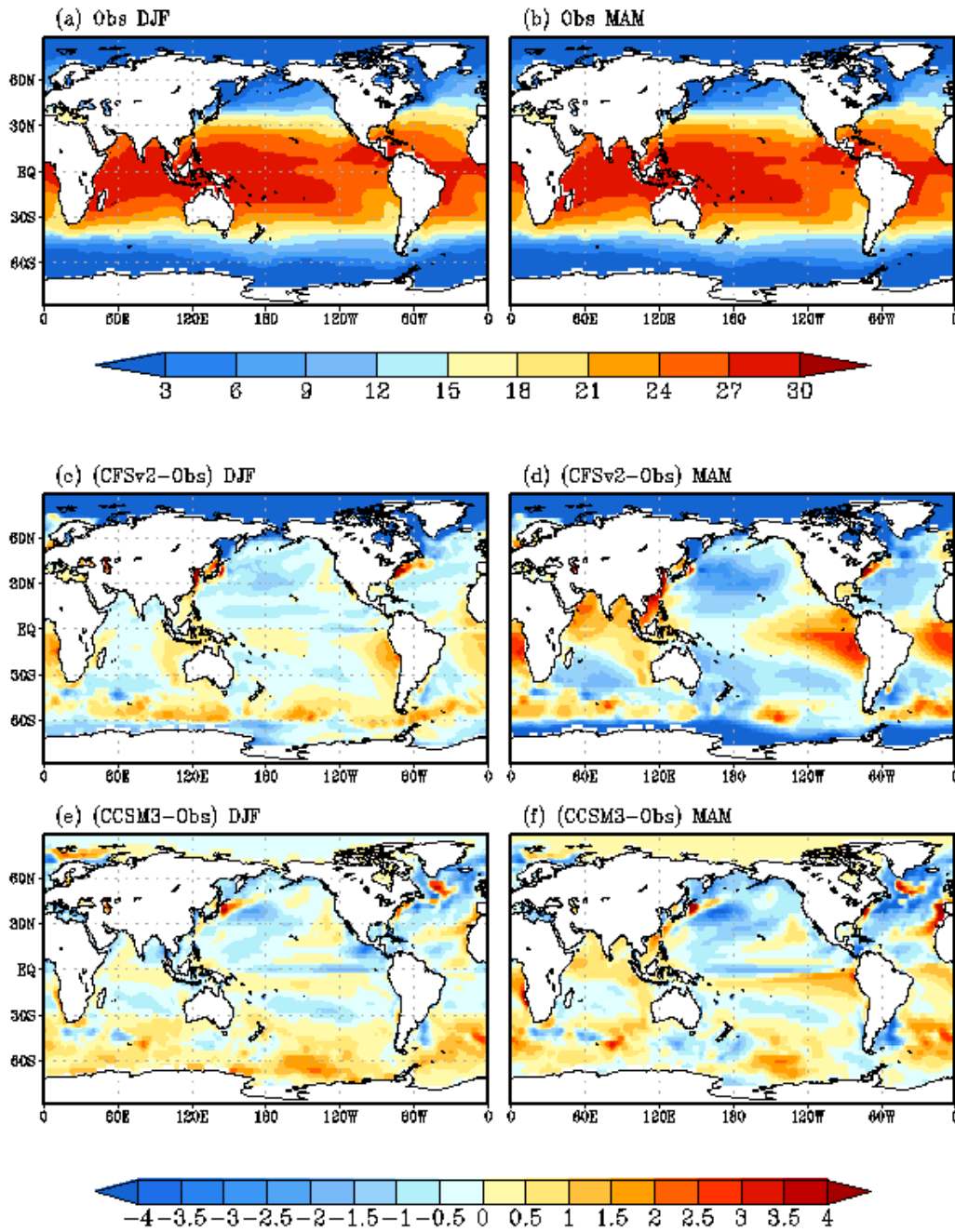


Figure 1. The observed climatological SST for boreal (a) winter (DJF) season and (b) spring (MAM) season. The bias of hindcasted SST at zero lead for boreal winter season from (c) CFSv2, (e) CCSM3. Similarly, the bias of hindcasted SST at one season lead for boreal spring season from (d) CFSv2 and (f) CCSM3.0. The units are in $^{\circ}\text{C}$.

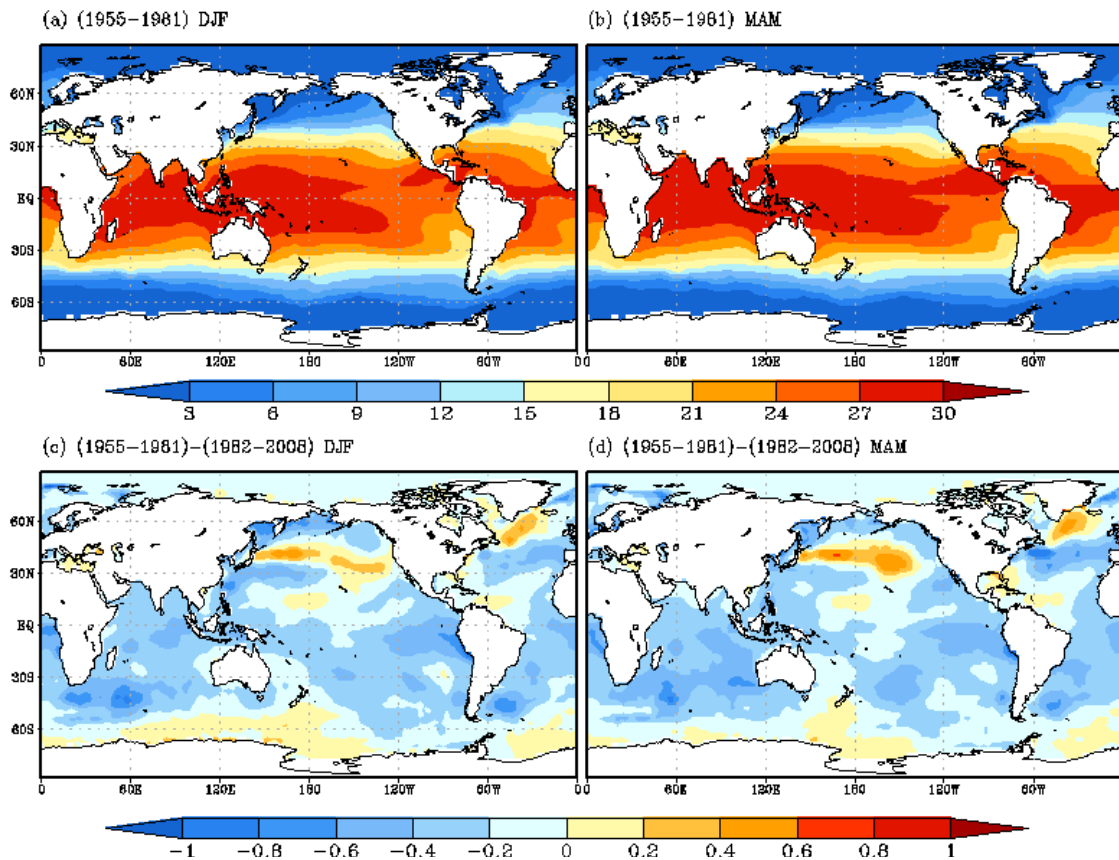


Figure 2. The observed climatology SST computed over a period of 1955-1981 for (a) DJF season and (b) MAM season, and their corresponding differences with climatology computed over the period 1982-2008 for (c) DJF and (d) MAM. The units are in $^{\circ}\text{C}$.

563

564

565

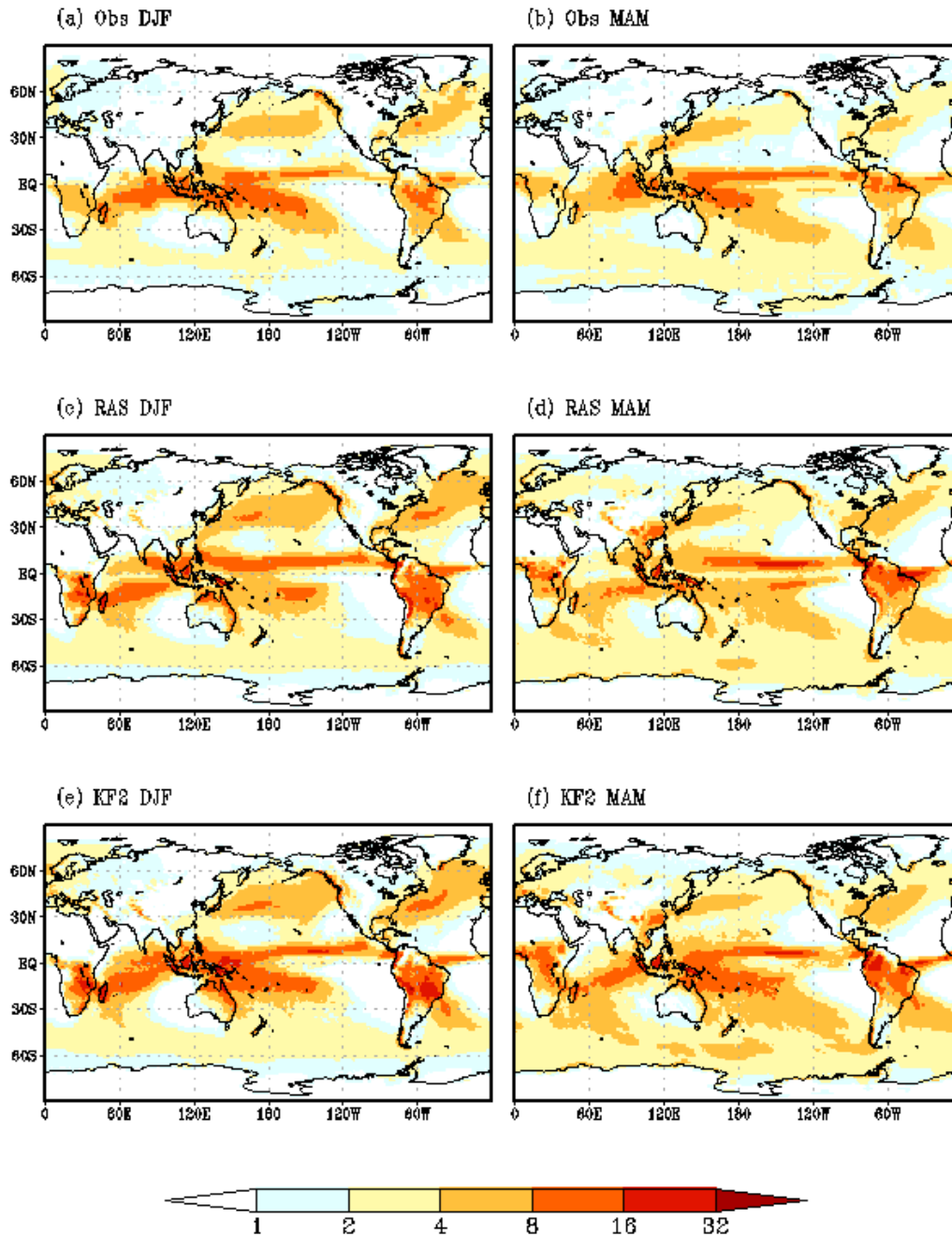


Figure 3. The observed climatology of precipitation computed over a period of 1982-1993 for (a) DJF and (b) MAM seasons. The corresponding climatology of precipitation from a single member seasonal hindcast for the period of 1982-1993 using the RAS convection scheme for (c) DJF (at zero lead) and (d) MAM (one season lead) season. Likewise the climatology of precipitation from a single member seasonal hindcast for the period of 1982-1993 using the KF2 convection scheme for (e) DJF (at zero lead) and (f) MAM (one season lead). The units are in mm/day.

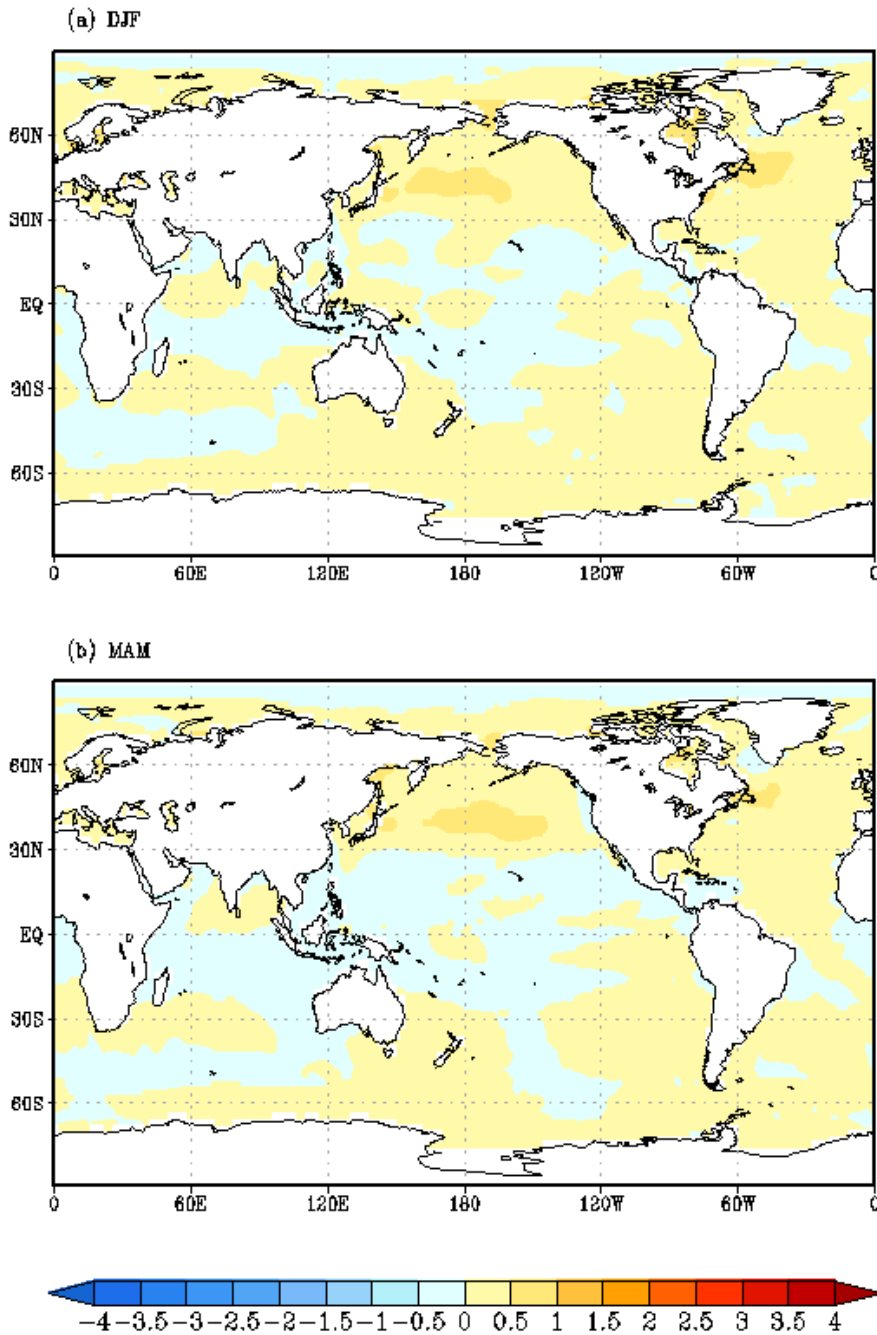


Figure 4. The climatological SST bias computed for (a) DJF season (at zero lead) and (b) MAM season (at one season lead) from FISH50. The observed SST climatology was computed over the period 1982-2008 as shown in Figs. 1a and 1b. The units are in $^{\circ}\text{C}$.

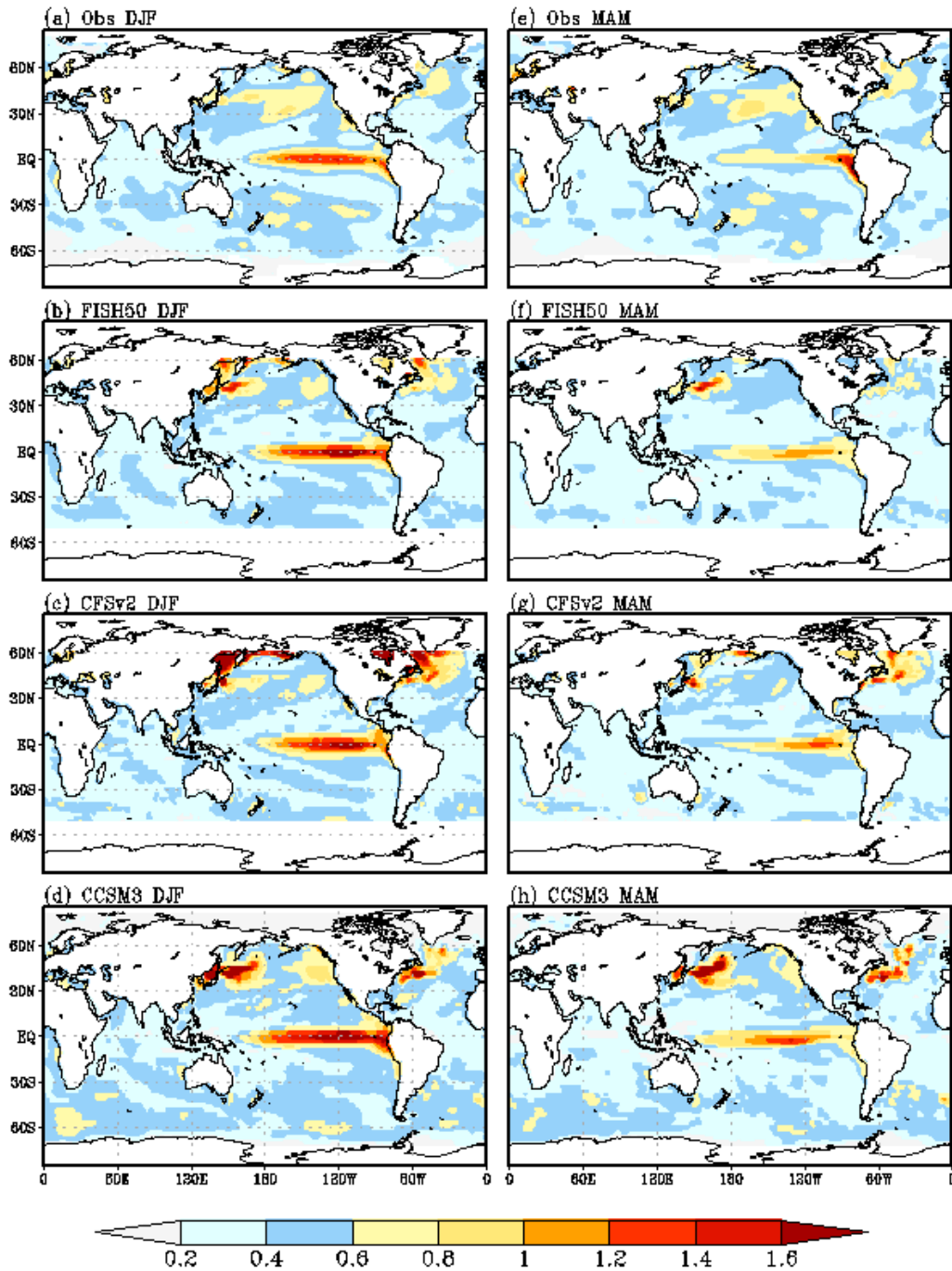


Figure 5. The standard deviation of DJF seasonal mean SST from (a) observations, and seasonal hindcasts at zero lead from (b) FISH50, (c) CFSv2, and (d) CCSM3. Similarly the standard deviation of MAM seasonal mean SST from (e) observations, and seasonal hindcasts at one season lead from (f) FISH50, (g) CFSv2, and (h) CCSM3. The units are in $^{\circ}\text{C}$.

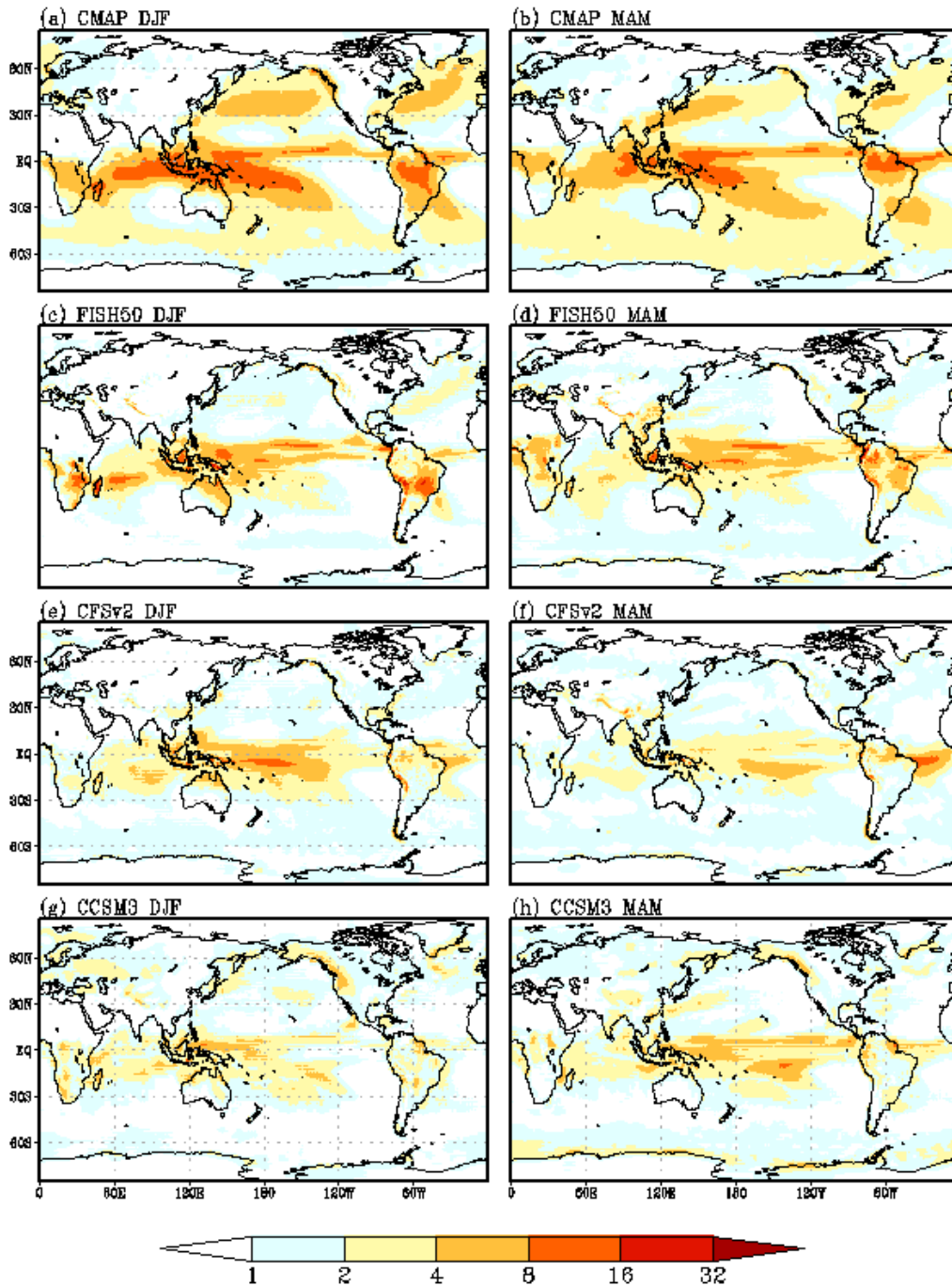


Figure 6. The observed climatology of precipitation (1982-2008) in (a) DJF, and (b) MAM. The root mean square error of the ensemble mean precipitation for DJF (zero lead) for seasonal hindcasts from (c) FISH50, (e) CFSv2, and (g) CCSM3. Likewise, the root mean square error of the ensemble mean precipitation for MAM (one season lead) for seasonal hindcasts from (d) FISH50, (f) CFSv2, and (h) CCSM3.

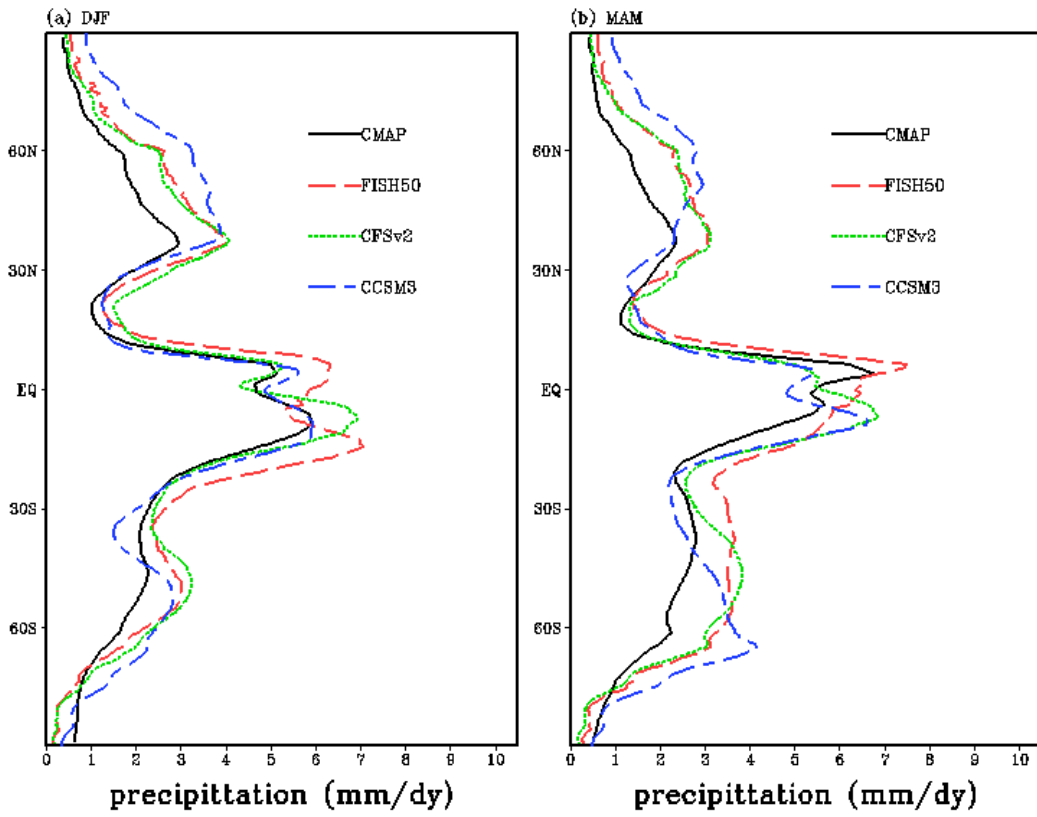


Figure 7. The zonal mean climatological (a) winter (DJF) and (b) spring (MAM) precipitation from observations and the three seasonal hindcasts.

574
575

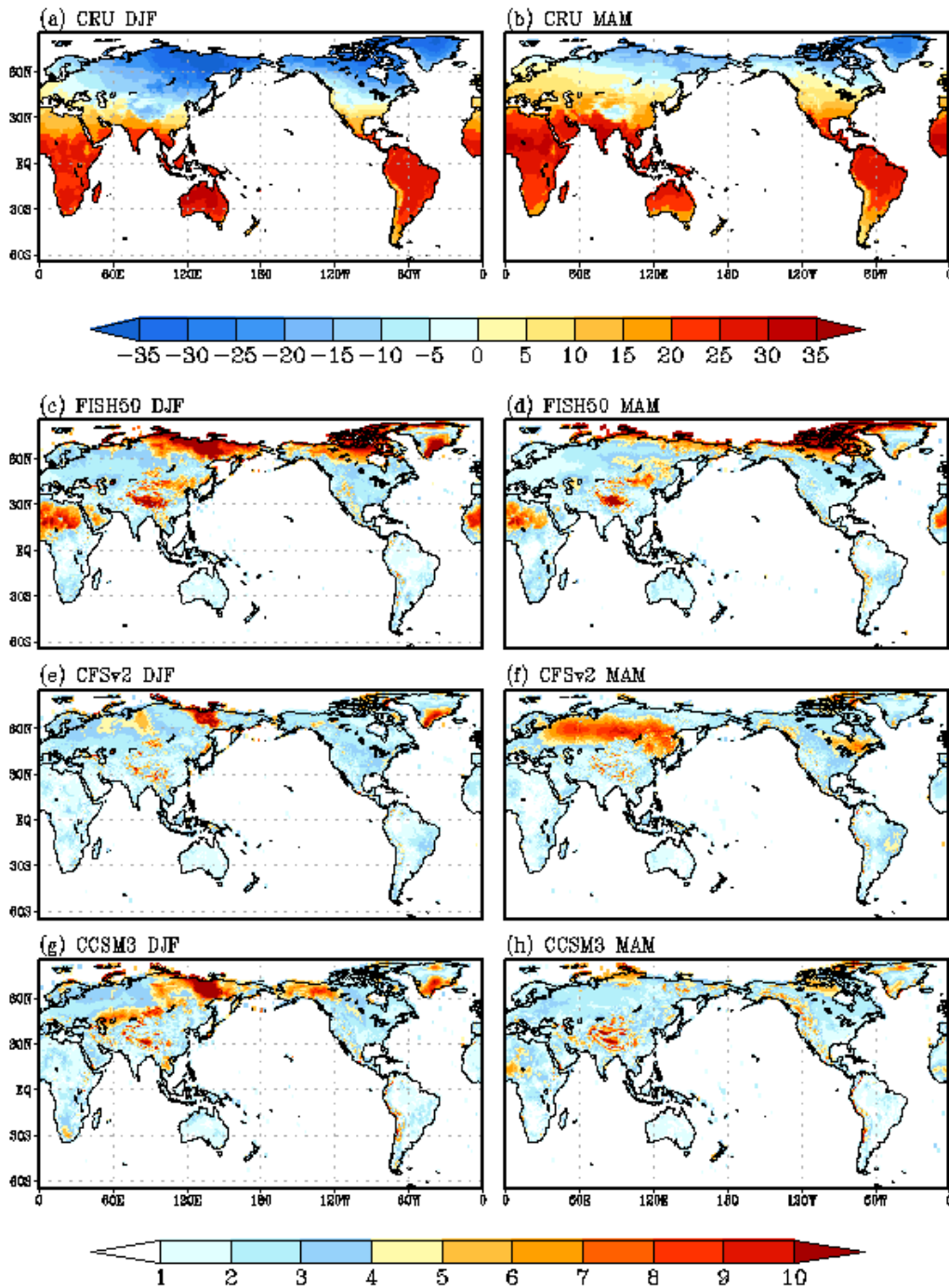


Figure 8. The observed climatology of surface temperature (1982-2008) in (a) DJF, and (b) MAM. The root mean square error of the ensemble mean T2m for DJF (zero lead) for seasonal hindcasts from (c) FISH50, (e) CFSv2, and (g) CCSM3. Likewise, the root mean square error of the ensemble mean T2m for MAM (one season lead) for seasonal hindcasts from (d) FISH50, (f) CFSv2, and (h) CCSM3.

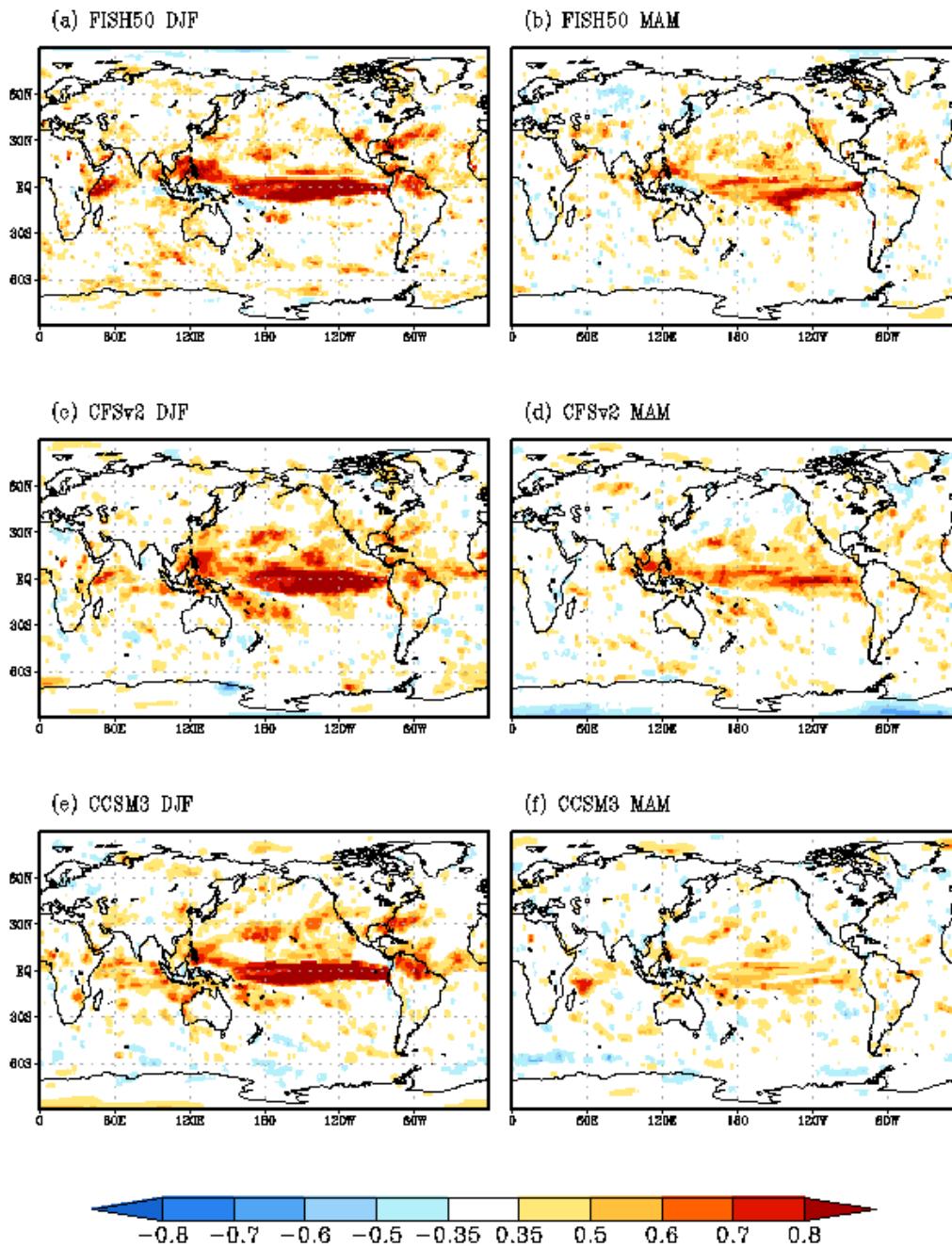


Figure 9. The correlation of the ensemble mean precipitation for DJF (zero lead) from (a) FISH50, (c) CFSv2, and (e) CCSM3. Similarly, the correlation of the ensemble mean precipitation for MAM (one season lead) from (b) FISH50, (d) CFSv2, and (f) CCSM3. Statistically significant correlations at 90% confidence interval according to the t-test are shown.

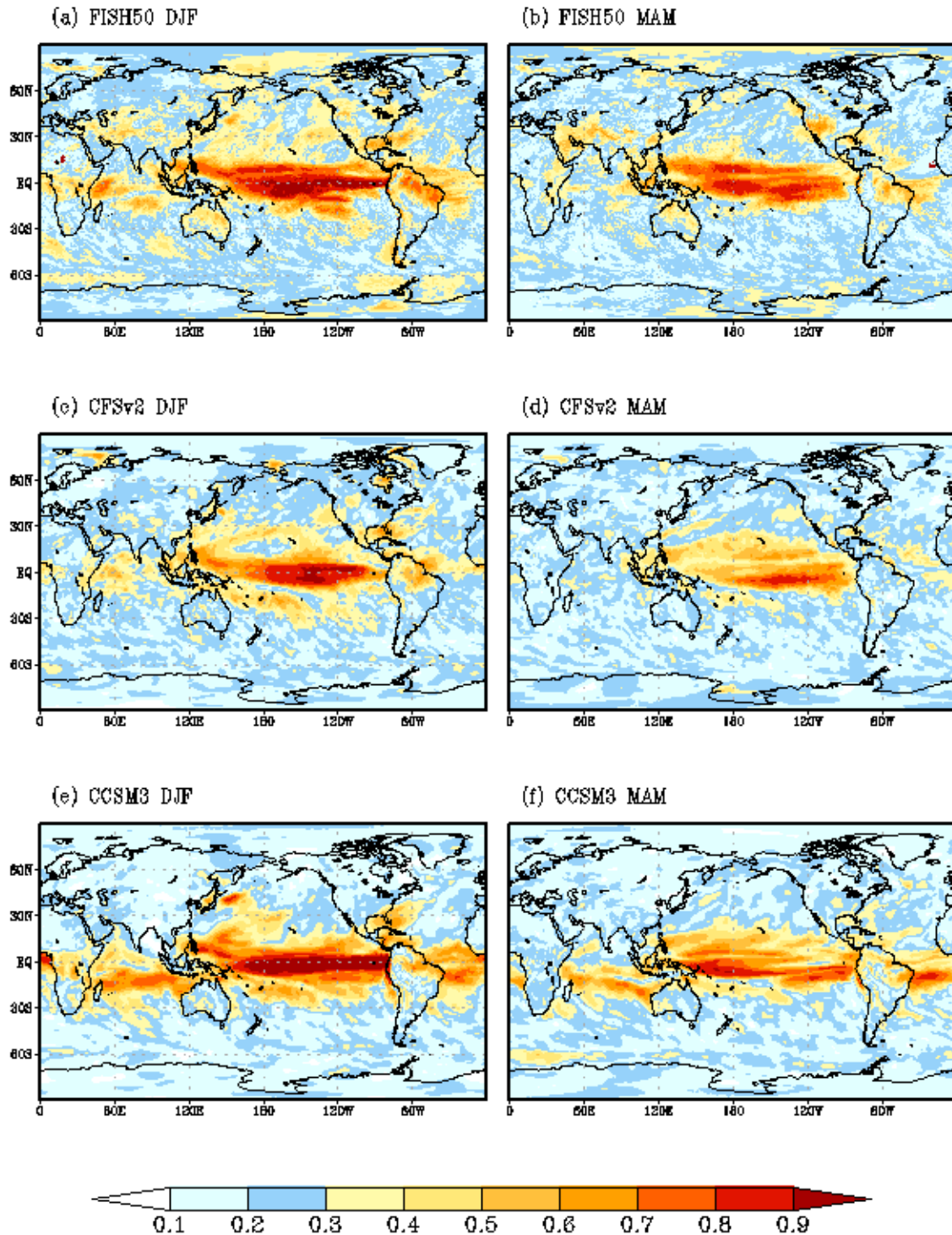


Figure 10. The signal to noise ratio of precipitation for DJF season (zero lead) for (a) FISH50, (c) CFSv2, and (e) CCSM3. The signal to noise ratio of precipitation for MAM (one season lead) from (b) FISH50, (d) CFSv2, and (f) CCSM3.

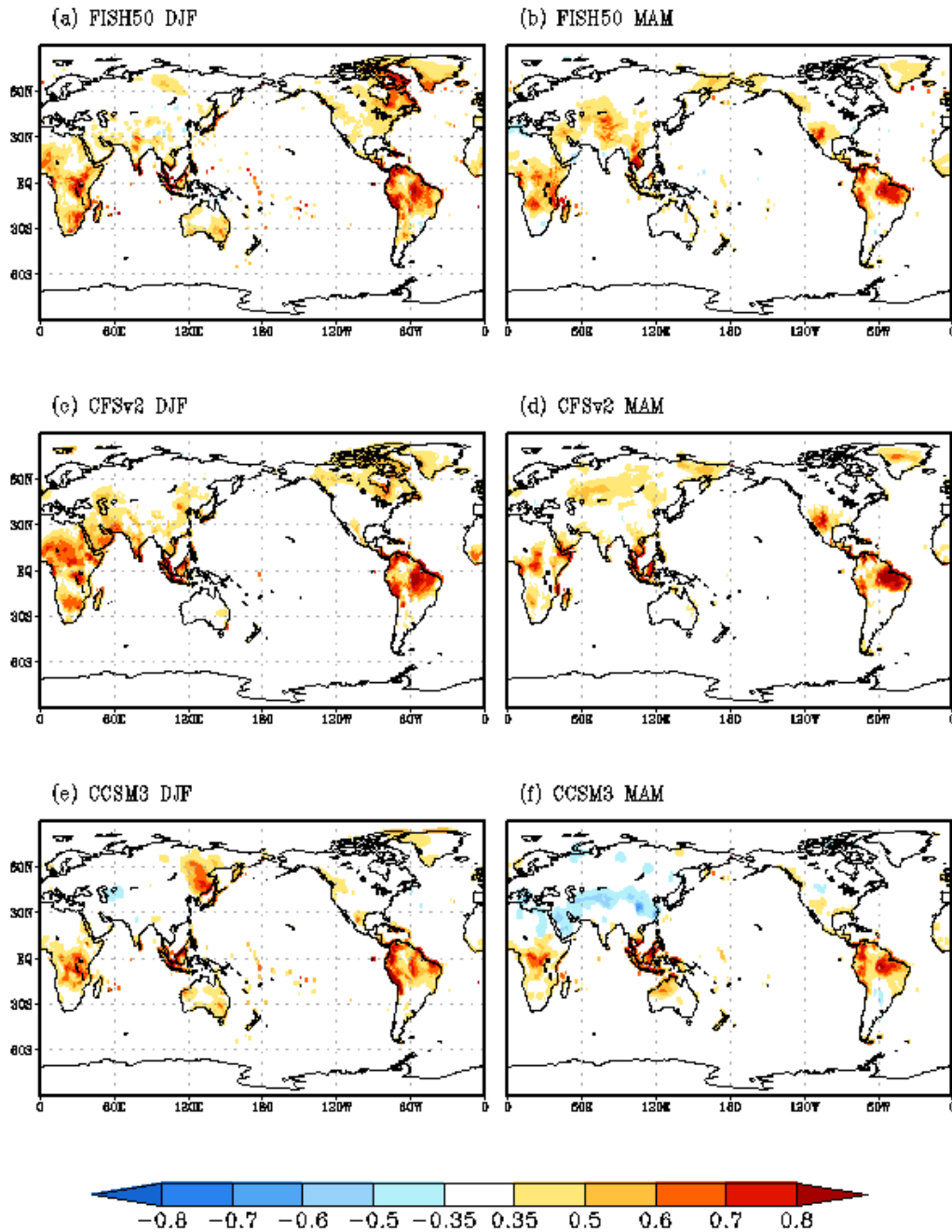


Figure 11. The correlation of the ensemble mean T2m for DJF (zero lead) from (a) FISH50, (c) CFSv2, and (e) CCSM3. Similarly, the correlation of the ensemble mean precipitation for MAM (one season lead) from (b) FISH50, (d) CFSv2, and (f) CCSM3. Statistically significant correlations at 90% confidence interval according to the t-test are shown.

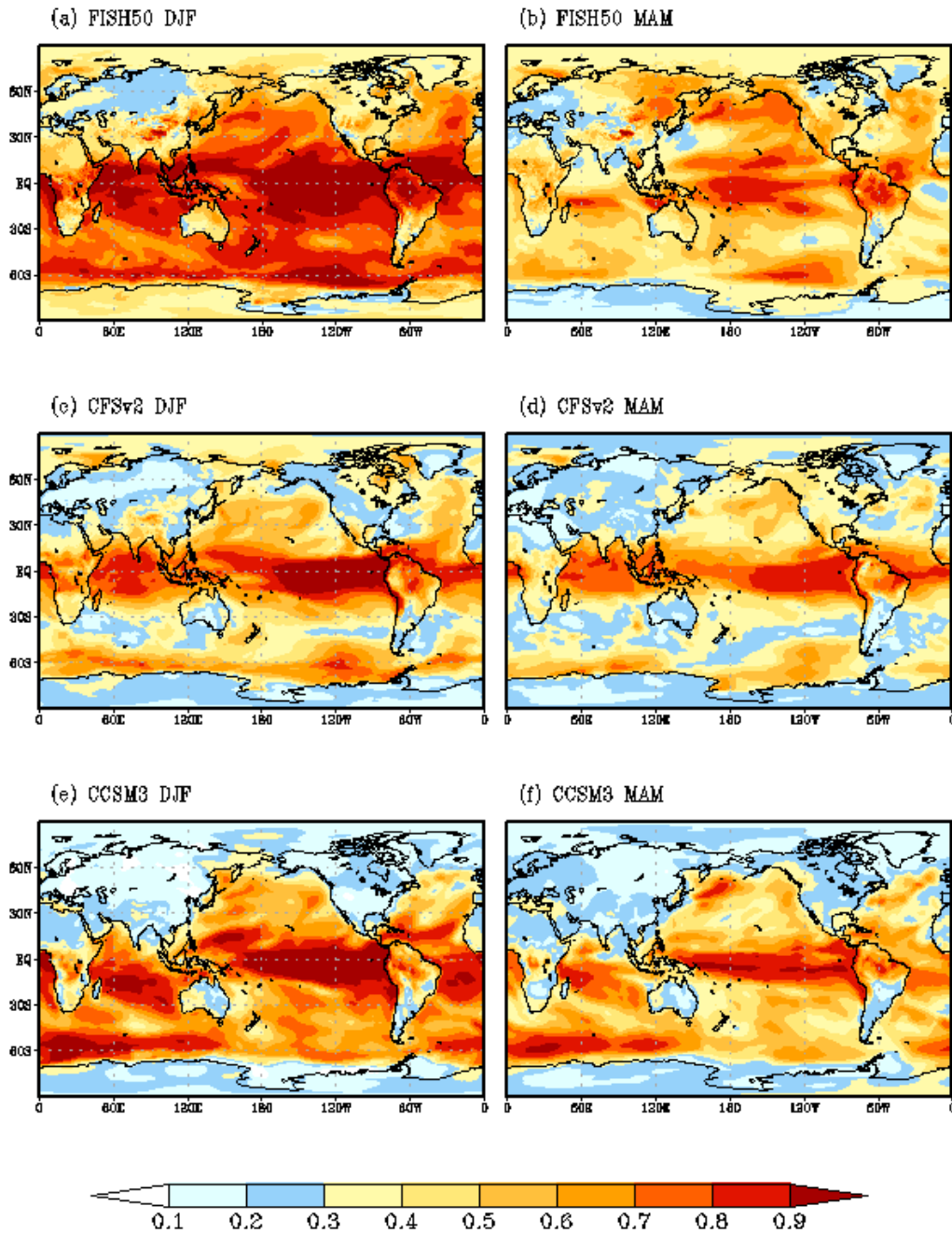


Figure 12. The signal to noise ratio of T2m for DJF season (zero lead) for (a) FISH50, (c) CFSv2, and (e) CCSM3. The signal to noise ratio of precipitation for MAM (one season lead) from (b) FISH50, (d) CFSv2, and (f) CCSM3.

584
 585
 586
 587
 588

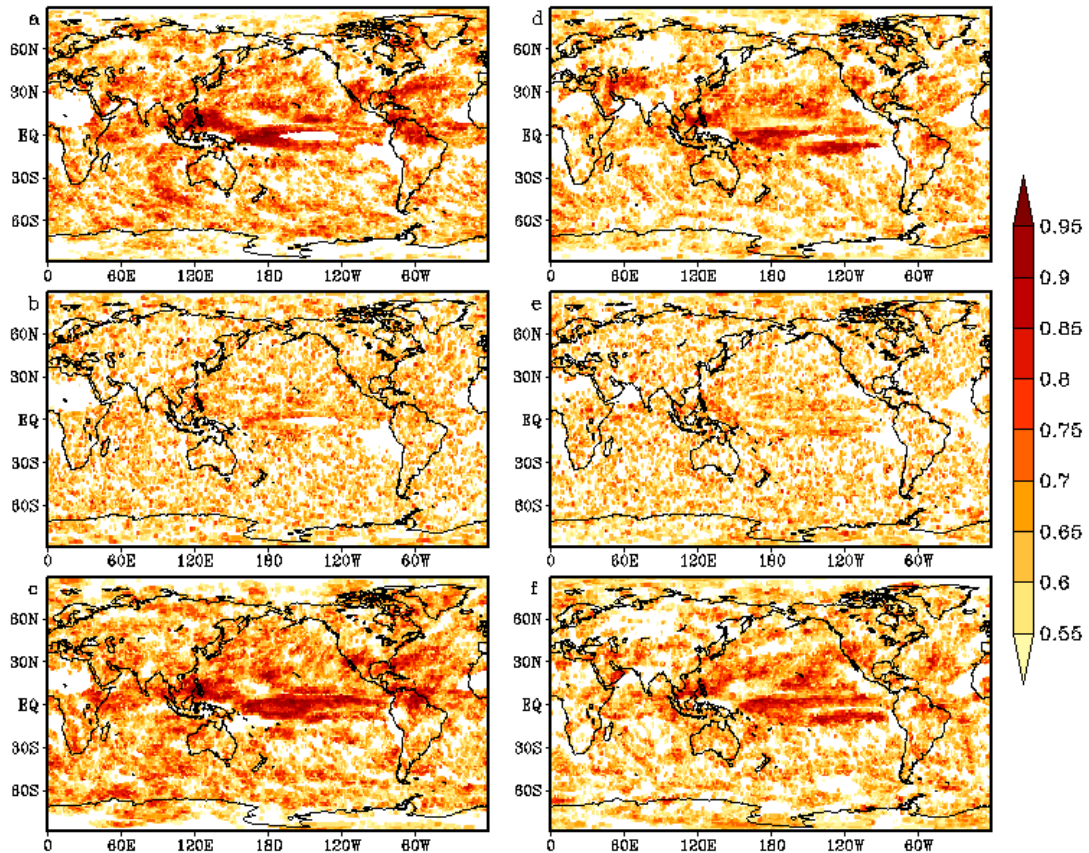


Figure 13. The area under the relative operation characteristic curve (AROC) for (a) lower, (b) middle, and (c) upper tercile for DJF (zero season lead) from FISH50 precipitation, Similarly, the area under the ROC for (d) lower, (e) middle, and (f) upper tercile for MAM (one season lead) from FISH50 precipitation. Area over 0.5 is colored and signifies higher skill than climatology.

589
 590
 591
 592
 593

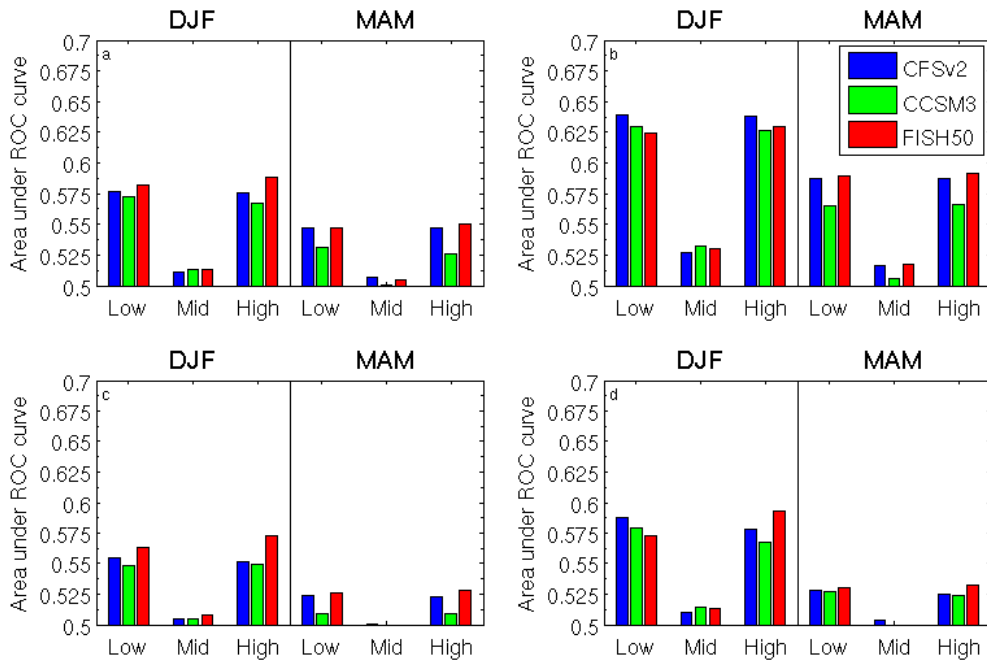


Figure 14. Area under the ROC averaged over (a) global oceans, (b) tropical oceans, (c) global land, and (d) tropical land for low, middle, and upper terciles of CFSv2, CCSM3, and FISH50 precipitation in DJF and MAM.

594
595
596

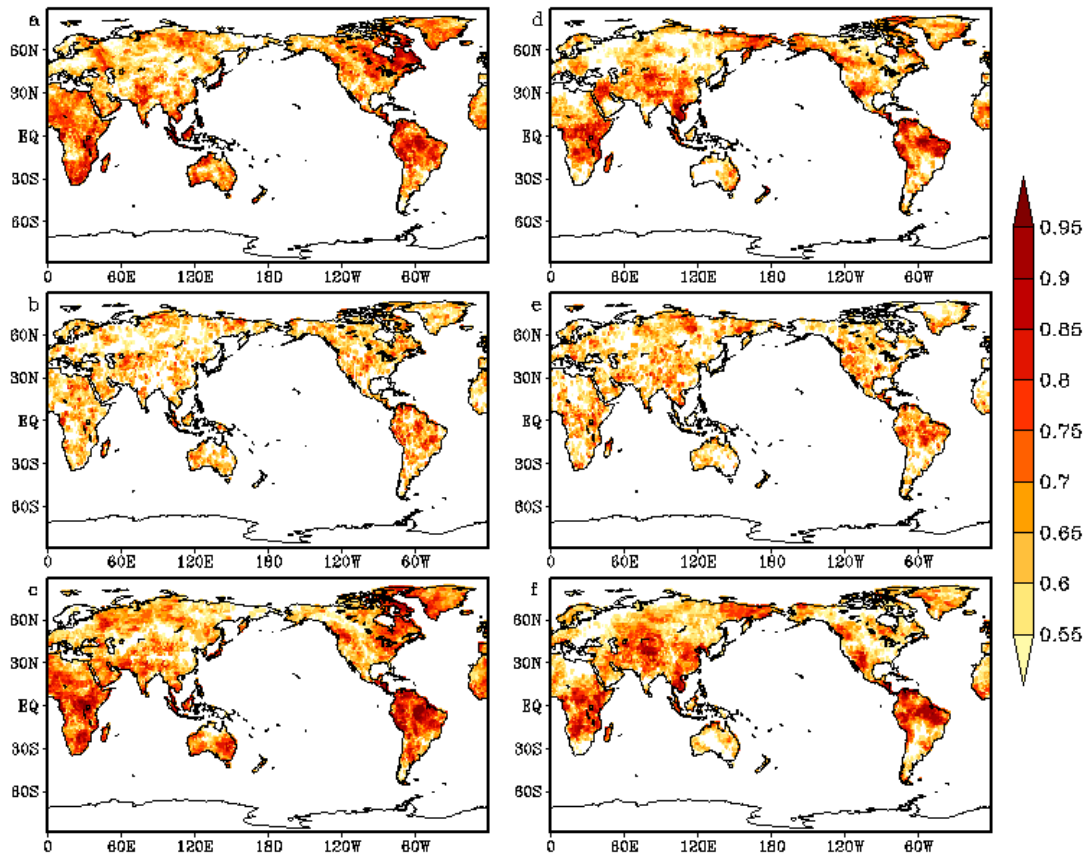


Figure 15. The area under the relative operation characteristic curve (ROC) for (a) lower, (b) middle, and (c) upper tercile for DJF (zero season lead) from FISH50 T2m. Similarly, the area under the ROC for (d) lower, (e) middle, and (f) upper tercile for MAM (one season lead) from FISH50 T2m. Area over 0.5 is colored and signifies higher skill than climatology.

597
 598
 599

599
600

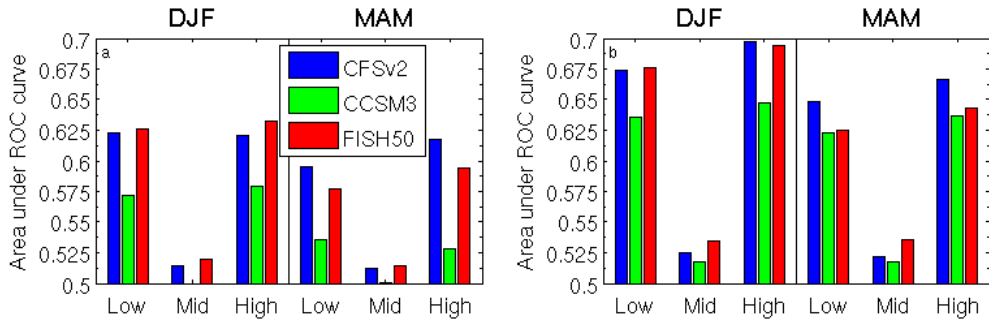


Figure 16. Area under the ROC averaged over (a) global land and (b) tropical land for low, middle, and upper terciles of CFSv2, CCSM3, and FISH50 temperatures in DJF and MAM.

601
602
603
604